Extreme Mechanics Letters 64 (2023) 102079

Contents lists available at ScienceDirect

Extreme Mechanics Letters

journal homepage: www.elsevier.com/locate/eml

Study of interwall interaction during the pull separation of ultra-long double-walled carbon nanotubes under lateral loading

Xuan Ye [b,a,1], Mengxiong Liu [f,g,1], Xide Li [c,d,*], Xiaoming Liu [b,e,**]

[a] Institute of Nuclear and New Energy Technology, Tsinghua University, Beijing 100084, China
[b] LNM, Institute of Mechanics, Chinese Academy of Sciences, Beijing 100190, China
[c] Department of Engineering Mechanics, AML, Tsinghua University, Beijing 100084, China
[d] Center for Nano and Micro Mechanics, Tsinghua University, Beijing 100084, China
[e] School of Engineering Science, UCAS, Beijing 100049, China
[f] College of Chemistry and Molecular Engineering, Peking University, Beijing 100871, China
[g] Beijing Graphene Institute (BGI), Beijing 100095, China

ARTICLE INFO

Article history:
Received 11 June 2023
Received in revised form 21 July 2023
Accepted 2 September 2023
Available online 9 September 2023

Keywords:
Carbon nanotubes
Interwall interaction
Buckling
Finite element simulation
Lateral pull-out

ABSTRACT

The successful fabrication of ultra-long carbon nanotubes (CNTs) makes CNTs ideal candidates for bearing systems due to the long sliding distance with low interwall interaction. However, it is difficult to measure the pull-out forces of ultra-long CNTs along their axes in real-time because of the difficulty of performing long-distance pull-out experiments. In this study, we proposed a lateral loading method to measure the interwall interaction force of ultra-long CNTs. By using a theoretical model and multi-scale finite element simulations, we could predict the interwall interaction force from the pull-out force in lateral loading. This pull-out force depends on the length of CNTs, and a critical length divides the pull-out force into two categories: maximum pull-out force due to local buckling and steady pull-out force due to sliding. In order to correctly measure the interwall interaction force by lateral loading, for the DWCNTs with the outer tube diameter of 0.955 nm, we have to make sure the lengths are greater than this critical value (54.2 nm) as experimental subjects.

1. Introduction

The exceptional behaviors of multi-walled carbon nanotubes (MWCNTs), carbon nanotube (CNT) fibers [1,2] and films [3], and CNT encapsulation [4] have attracted widespread attention of researchers. MWCNTs are composed of coaxial cylindrical graphene walls with an approximate wall spacing of 0.34 nm [5,6], where the interwall interaction is dominated by weak van der Waals (vdW) force rather than chemical bonds. Therefore, the walls tend to slide or rotate easily against the others under the action of external axial forces [7–9], which makes the MWCNTs an ideal candidate for ultrahigh-frequency longitudinal oscillators in nano-electro-mechanical systems (NEMS) [10,11].

For short CNTs with a length of micrometer or nanometer, the pull-out experiments were generally performed along the axial direction of the tube to obtain the interwall interaction force. The measurement method of pulling the inner tube out of the outer tube along the axial direction is straightforward and the measurement result is clear. Cumings et al. [8] proposed a "telescoping" extension mode and measured the pull-out force of 9.1 nN. Yu et al. [12,13] proposed a "sword-in-sheath" failure mechanism, measured the pull-out force of 10 nN by soft and hard probes stretching, and found the pull-out force had a constant background with superimposed abrupt dissipation events ranging from 0.3–3.1 nN [14]. For micron-long CNT bundles (CNTBs), the measured normalized force per CNT-CNT interaction was 1.7 ± 1.0 nN when an inner bundle of double-walled carbon nanotubes (DWCNTs) was pulled out from an outer shell of DWCNTs [15]. For centimeter-long DWCNTs, the macroscopic superlubricity was observed [16], where the interwall friction force (<5 nN) was independent of the pull-out length, but linearly dependent on the pull-out velocity of the inner wall and affected by the axial curvature [17]. Moreover, to improve the fracture toughness of CNT/polymer nanocomposites, the interfacial interaction between CNTs and the polymer is investigated by conducting the pull-out experiments, where the pull-out speed and the bonded/non-bonded interactions are focused [18,19]. Meanwhile, theoretical and numerical [20–23] studies were carried out to understand the axial pull-out process and sliding behavior of the MWCNTs. The interwall interaction of DWCNTs

* Corresponding author at: Department of Engineering Mechanics, AML, Tsinghua University, Beijing 100084, China.
** Corresponding author.
E-mail addresses: lixide@tsinghua.edu.cn (X. Li), xiaomingliu@imech.ac.cn (X. Liu).
[1] These authors contributed equally to this work.

https://doi.org/10.1016/j.eml.2023.102079
2352-4316/

was mainly derived from the end of the wall and proportional to the diameter of the critical wall [9], while independent of the overlap area/length and chirality [24], but closely related to the sliding velocity [24,25], temperature [26], and defects [27–29].

However, for ultra-long CNTs with lengths on the order of centimeters [30,31], their length-to-diameter ratio can reach 10^7. It is difficult to conduct long-distance pull-out experiments along their axial direction with the pull-out force monitored in real time. There are two main reasons. On the one hand, present micro/nanomanipulators with nanoscale displacement accuracy have limited travel, such as the Kleindiek micro/nanomanipulator (MM3A-EM, Kleindiek Nanotechnik GmbH, Reutlingen, Germany). When the displacement is large, the micro/nanomanipulator moves in an arc. On the other hand, mostly atomic force microscope (AFM) probes or nanowires with known stiffness (K) are used as cantilever sensors for the measurement of pull-out forces on the nano-Newtown scale. During the force measurement, the cantilever deflection (δ) is recorded using the image of the microscopic observation system, and then the force of the sensor is calculated as $F = K\delta$. Nevertheless, it is difficult to meet the requirements of high accuracy and wide field of view of the microscopic image at the same time.

Therefore, we developed a new experimental method to measure the interaction forces between the inner and outer tubes of ultra-long carbon nanotubes. We used a string tension-like method [30,32] by laterally loading the span of the ultra-long carbon nanotube to cut the outer wall (Fig. 1). When the outer tube breaks, the inner tube adsorbs to the surface of the probe tip (Figs. 1a and 1b). The inner tube is laterally pulled out from the outer tube, and the lateral force–displacement curve is recorded. This method is very effective for specimens with large slenderness ratios, and can be applied to optical and scanning microscope platforms. In particular, it can be applied directly to a suspended specimen on a silicon substrate groove. Tensile and bending experiments are performed directly on micro/nanoscale specimens, avoiding the need to transfer them to specific measurement devices through complex and difficult procedures. For example, we and our collaborators have applied this experimental method to the studies of tensile properties of ultra-long CNTs [30], the interaction between carbon nanotubes/walls in the bundle/tubes [31], fatigue properties of CNTs [33], the strength and toughness of CNTs [29].

Although this experimental method is effective in previous studies, there are still some issues worth discussing to make it a reliable and controllable measurement platform for special specimens. (1) The influence of the lateral loading method on the measurement results of inter-wall forces is uncertain, especially for the bending behaviors of CNTs which is the main factor caused by the lateral loading. (2) The details of carbon nanotube deformation are hard to capture due to the limited load resolution and image spatial resolution of the experiment. (3) Assuming that the vdW shear force (f) is independent of the overlap length [17] and the inner tube approximates as a soft string (with a high aspect ratio$\sim 10^7$), a mechanical equilibrium analysis of the inner tube (as illustrated in Fig. 1c) is conducted. The relationship between the lateral force (F) and the lateral displacement (y) can be derived as $F = 2f\frac{y}{\sqrt{y^2+(L/2)^2}} = 2f\frac{1}{\sqrt{1^2+(L/2y)^2}}$, where L is the initial length of the nanotube. As y increases, lateral force F should increase from $2f\frac{1}{\sqrt{1^2+(L/2y_0)^2}}$ to $2f$, where y_0 is the initial position of DWCNTs at the time of outer wall fracture (Fig. 1c). However, no such trend was observed in the experimental lateral force–displacement curve (the red box in Fig. 1d).

This paper mainly used numerical simulation and theoretical analysis method to study the mechanical response of CNTs under lateral loading, and focused on the scope of applicability of

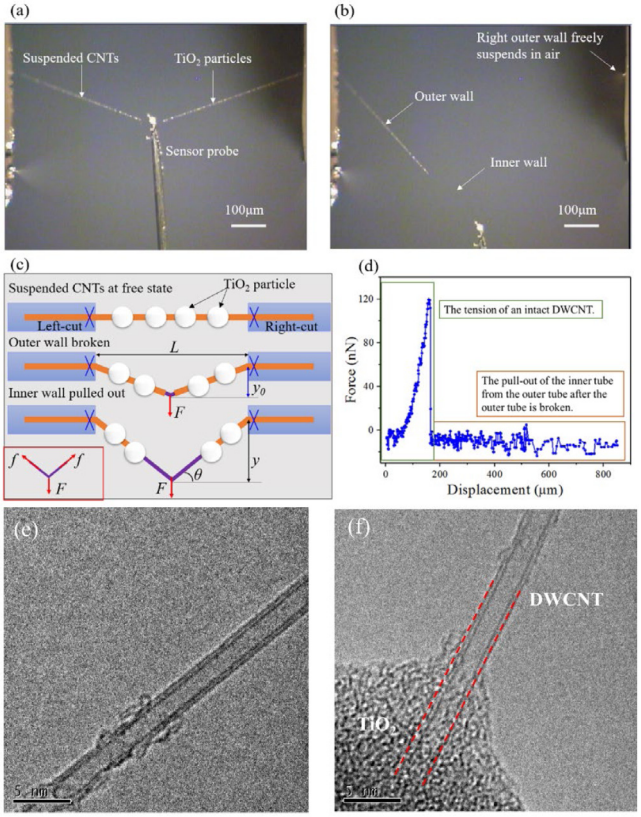

Fig. 1. The experimental results [31], (a-b) photograph and (c) schematic for an inner wall pulled out from an outer wall under lateral force with both ends of DWCNT cut [17], (d) corresponding lateral force–displacement curve, including two stages: the tension of the intact DWCNT and the inner wall pulled out from the outer wall after rupture of the outer wall, (e) TEM image of DWCNTs, (f) TEM image of DWCNTs decorated by the TiO_2 particle.

the measurement method of lateral loading. Firstly, for DWCNTs with short length (tens of nm), the MD model was developed to simulate the pullout process of the inner tube from the outer tube. Then, for longer carbon nanotubes (L > 60 nm), a finite element model that can be extended to the macroscopic scale was established due to the limitation of computational power and computational cost of MD. Finally, through theoretical modeling, the carbon nanotube length requirements for accurate measurement of the interwall interaction force using the lateral loading method were obtained. And then we developed a theoretical model to predict the critical buckling force and the stable force. In addition, to illustrate the effect of the lateral loading on the measured pull-out force, we also investigated the variation law of the lateral force–displacement curve, the corresponding mechanism, and the length effect of nanotubes under lateral loading. These findings may shed light on designing micro-nano devices with ultra-low interwall interaction.

2. Methods

2.1. Experimental method

The ultra-long CNTs were prepared through a gas-flow -directed chemical vapor deposition (CVD) method and suspended on a silicon substrate (with a 500 nm thick SiO_2 layer on the surface). The nano sized TiO_2 particles (e.g., white beads in Fig. 1a) were decorated on the CNTs surface by vdW force for optical visualization [34]. Transmission Electron Microscope (TEM) images in Fig. 1 showed that the CNTs were double-walled with

the outer tube diameter ranging from 2 nm to 3 nm [29–31]. The micro/nanoscale mechanical test system (m/n-MTS) was used to investigate the interwall interaction [32,35]. The displacement resolution of the translation stage is 0.5 nm and the resolution of micro-force sensing probe is 5 nN (FT-S100, FemtoTools, Switzerland). Based on the micro/nanoscale mechanical test system [32,35], the DWCNTs were slowly stretched. Until an abrupt separation of two adjacent TiO_2 particles was observed, while the spacing of the TiO_2 particles at other locations remained almost unchanged (Fig. 1b). After the outer wall breaks, the inner wall is continuously pulled out (Fig. 1c). Moreover, to eliminate the effect of the ultra-long DWCNTs ends on its interwall interaction force, we scratched the ends of the suspended carbon nanotubes using a probe before experiments. The lengths of the inner and outer tubes were made to be consistent with the substrate gap distance. The specific scribing method has been reported in our co-authors' study [17].

Since the TiO_2 particles are only attached to the surface of the outer wall, they can be used as a marker for the position of the outer wall. As there is no mark on the surface of the inner wall, they are not visible in Fig. 1a. Moreover, the TiO_2 particles decorated on the surface of outer tube of DWCNTs do not affect the pullout experiment and sliding of CNTs. The specific reasons include three aspects: (1) It shows that the interaction between TiO_2 particles and CNTs is dominated by van der Waals interaction, which is much lower than the mechanical strength of CNTs and has no impact on the mechanical strength of CNTs [23,24]. (2) From Fig. 1 of the pullout experiment, it can be seen that the number of nanoparticles on the outer tube as well as the distance between neighboring nanoparticles remain unchanged when the inner tube is continuously pulled out and pulled up to several hundred micrometers. This indicates that TiO_2 particles are adsorbed only on the surface of the outer tube of the DWCNT. (3) The diameter of the outer tube of the DWCNT is about 2 nm, and the TEM image in Fig. 1f shows that the TiO_2 particles did not cause axial and radial deformation of the carbon nanotube. Due to the decoration of the TiO_2 particles, the position of the inner wall can be judged by the relative position of the force sensor tip and the outer wall, as shown in Figs. 1a and 1b. When the inner tube is pulled out from the outer tube, a triangular configuration is formed between the outer tube and inner tube (Fig. 1a). When the inner tube breaks or the inner tube is completely pulled out from the outer tube, the outer tube freely suspended in the air (Fig. 1d). Eventually, the entire carbon nanotube structure will adsorb to the silicon substrate or force sensor tip to maintain the minimum potential energy.

In this way, the entire extraction process of the inner wall can be monitored. The lateral force–displacement curve (Fig. 1d) and lateral pullout force–displacement curve after the outer tube rupture (red box in Fig. 1d) were obtained. The force sensor shows a lateral force of 120.0 nN and lateral displacement (y_0) of 164.7 μm before the outer tube broke. And then the inner tube was continuously pulled out and the force dropped to near zero. Moreover, more detailed information about the experimental results can be obtained from the Ref. [31].

2.2. Molecular dynamics simulation

The previously measured pull-out force of DWCNTs along the tube axis was about 1–4 nN, depending on the diameter of the outer wall, regardless of the overlap length of the inner and outer walls [36,37], while the lateral pull-out process of the inner wall from a DWCNTs was rarely studied.

Considering that the CNT is virtually formed by curling the graphene sheet, the geometry of the CNT is specified by the integers (n, m) depending on the way the graphene sheets are curled. The diameter of the nanotube (n, m) is given by $d = \frac{\sqrt{3}a}{\pi}\sqrt{n^2 + nm + m^2}$, where a is the bond length of C–C. Here, an MD model of (5,5)/(10,10) DWCNTs with a length of 30 nm was built, where the center of the outer wall was truncated (Fig. 2). (5,5) and (10,10) are the inner and outer tubes of the DWCNTs. Both ends of the outer wall are fixed in all directions, similar to the fixed boundary condition used in continuous theory. The center of the inner wall is loaded laterally at a constant speed of 20 m/s.

The details of the simulation of the successive pull-out process of the inner tube against the outer tube are described as follows. MD simulations were carried out using open sources LAMMPS (Large-scale Atomic/Molecular Massively Parallel Simulator). The Adaptive Intermolecular Reactive Empirical Bond Order (AIREBO) potential [38], allowing for the C–C bond breaking and forming, was selected to describe the C–C bonded interaction because it compared reasonably well to first-principles predictions and successful in describing the intermolecular interactions in carbon and hydrogen materials [39,40]. The Lenard-Jones (LJ) potential [41] with $\varepsilon = 0.00284$ eV, $\sigma = 0.34$ nm, and a cut-off distance of 1.0 nm was applied to describe the vdW non-bonded interactions between the inner and outer tubes. The NVE (constant Number of atoms, Volume, and Energy) ensemble was adopted with the temperature controlled around 0.01 K and the Verlet algorithm was employed with a time step of 0.5 fs.

2.3. Finite element method

According to the model of MD, a finite element model with corresponding dimensions was built, including the inner tube, the outer tube, and the sensor tip shown in Fig. 3. The inner and outer tubes are modeled and simulated using shell elements, where the element types are all S4R with a mesh size of 0.1 nm. The sensor tip was modeled and simulated using an analytic rigid body due to its high stiffness, and its motion was controlled by a reference point with 6 degrees of freedom. Due to symmetry, a 1/2 model was developed to improve computational efficiency. The commercial finite element software package Abaqus/Explicit was used to solve the finite element process. The linear-elastic model is used for the nanotubes with material parameters as follows. Young's modulus is 5.15 TPa and Poisson's ratio is 0.19 for the effective mechanical wall thickness of 0.066 nm [42]. Reasons for choosing these parameters are as follows. In fact, the elastic constant is the mechanical concept under the framework of the continuous medium, while CNT is the discontinuous structure with the single atomic layer. Thus, the effective thickness must be assumed to be continuous before it becomes meaningful. The parameters with the Young's modulus of 1 TPa and the effective thickness of 0.34 nm can effectively describe the in-plane deformation of CNTs according to the previous work [29,43]. However, the bending and buckling behavior of CNTs mainly depends on the bending characteristics of graphite plates. For a plate, the bending stiffness is used to describe the bending properties in the continuous media and the expression of the bending stiffness of a plate is shown below. It was found that if the Young's modulus of 1 TPa and the effective thickness of 0.34 nm were used, the calculated bending stiffness was nearly 25 times larger than the effective bending stiffness of 0.85 eV [42], which created a contradiction. According to the research of Yakobson [42], the bending stiffness defined under the framework of continuous medium was applicable to CNTs when the effective thickness was 0.066 nm. Thus, for the bending characteristics of the CNTs, the parameters with the Young's modulus of 5.15 TPa and the effective thickness of 0.066 nm are selected to ensure the harmonization.

Fig. 4 shows the loads and boundary conditions. The boundary conditions mainly consisted of two parts, including a fixed

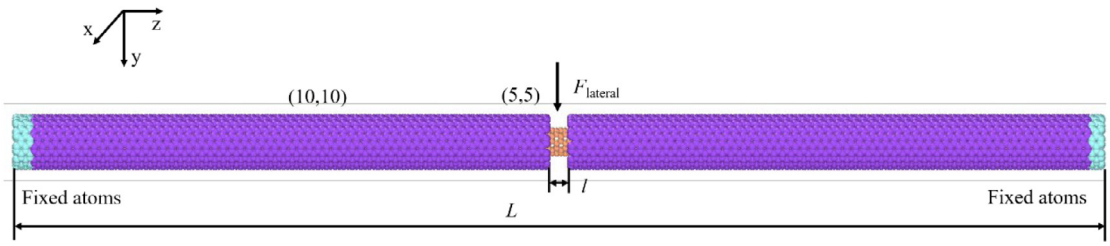

Fig. 2. Schematic diagram of the MD model for (5,5)/(10,10) DWCNTs with a length of 30 nm loaded laterally.

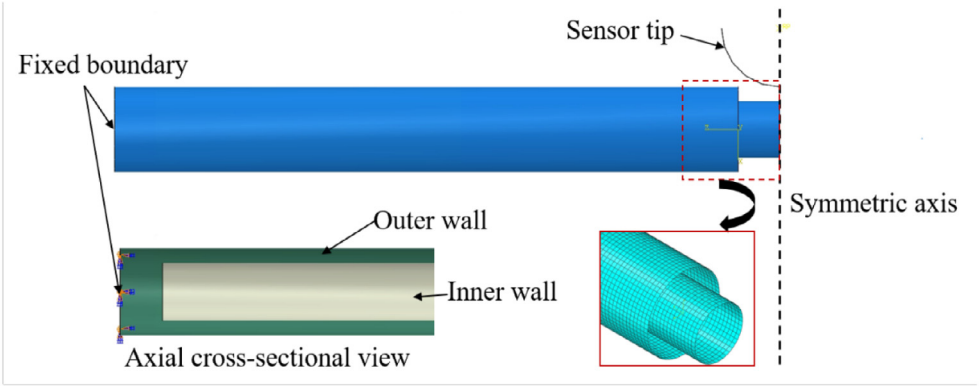

Fig. 3. The symmetric finite element model of a (5,5)/(10,10) DWCNTs under lateral loads. The diameters of the inner and outer tubes are 0.678 nm and 1.356 nm, respectively.

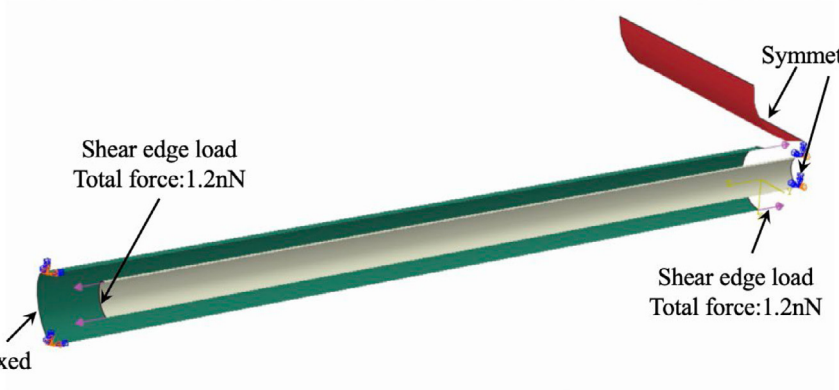

Fig. 4. Schematic diagram of loads and boundary conditions.

boundary condition imposed on the end of the outer tube and a symmetric boundary condition imposed on the symmetry plane of the 1/2 model. The load is a given displacement applied at the reference point of the sensor tip until the inner tube is pulled out. For the contact behavior, it mainly includes the normal and tangential forces. The tangential force, as discussed in Fig. 8, it is a distributed force with a total of 1.2 nN applied to the left end of the inner tube and the right end of the outer tube due to the interaction of the inner and outer tubes during the pull-out process. For the normal force, it adopts the "soft contact", and the displacement-pressure relationship satisfying the L-J potential shown in Fig. 6 is defined by inputting the normal contact force-overclosure curve to the FEM.

3. Results and discussions

3.1. Simulations of the pull-out process under lateral loading by MD

Fig. 5a shows the lateral force–displacement and total potential energy-displacement curves for (5,5)/(10,10) DWCNTs with a length of 30 nm. They both consist of two stages: Stage I and Stage II. Fig. 5b shows the corresponding overall geometric changes. In Stage I, the system's potential energy and displacement approximately satisfy a quadratic relationship, indicating that both the inner and outer tubes exhibit uniform elastic bending. All the work done by the external force is converted into the strain energy of the system. The cross-section of the entire structure remains circular.

When the lateral force increases to the peak value of 4.34 nN, it suddenly decreases until stabilizes near a certain value and exhibits no significant change with the increase of displacement (into Stage II). At the same time, the potential energy-displacement curve changes from nonlinear to nearly linear (Fig. 5a). Two local snap buckles appeared near the two ends of the outer wall (Fig. 5b). The cross-section of the outer wall changes from circular to elliptical, releasing energy through partial collapse (Fig. 5b). After that, the two buckling sections on the outer wall are transformed into two hinges. The inner wall is then pulled out stably with a lateral force of about 2.49 nN (stable lateral force).

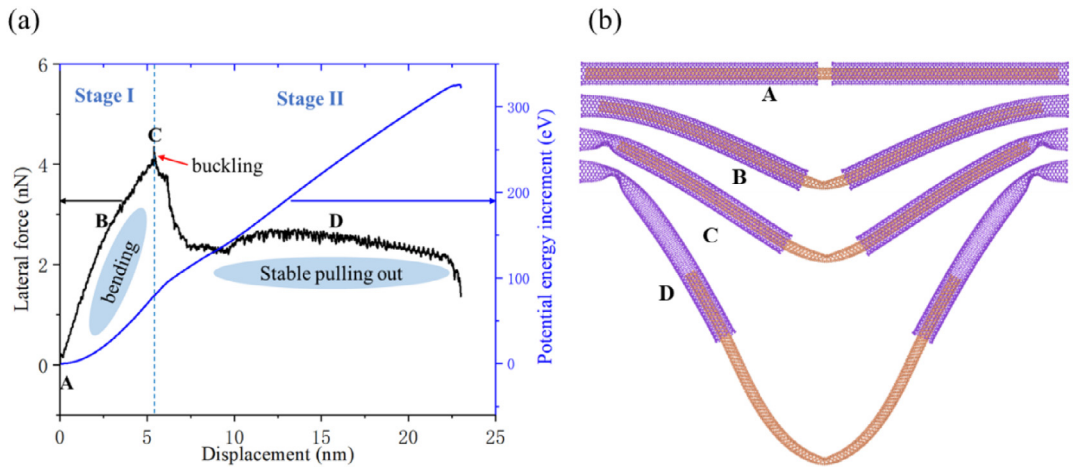

Fig. 5. MD results. (a) Lateral force–displacement and potential energy increment-displacement curves, and (b) typical geometric changes of (5,5)/(10,10) DWCNTs with a length of 30 nm.

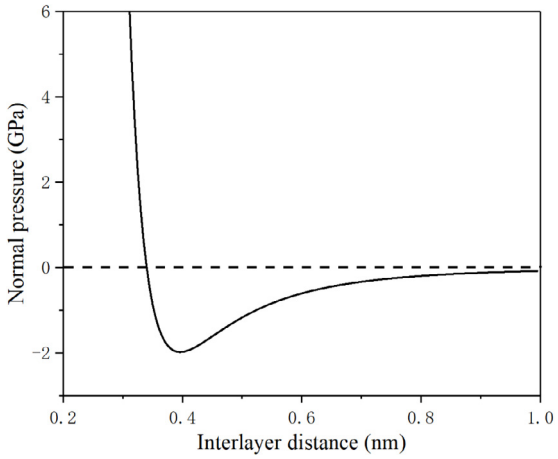

Fig. 6. Relationship between the interlayer pressure and interlayer distance.

3.2. Lateral pull-out of DWCNTs by FEM

MD method can effectively simulate the deformation of DWCNTs under lateral loading. However, the computational expense of MD simulations limits the length of DWCNTs that can be studied. Here, FEM is used to simulate the lateral pull-out of longer nanotubes. Before this, some reasonable equivalence of the interactions between the inner and outer tubes is required, including the stiff vdW normal interaction and the compliant shear interaction. By simulating the proximity of two graphene sheets with MD, a pressure-distance curve can be obtained. For this simulation, the in-plane geometry of the graphene sheets was kept fixed, just changing the interlayer distance. The relationship between the normal pressure and interlayer distance was obtained (Fig. 6). Pantano et al. [44] pointed out that this equivalence was also applicable to surfaces with different radii of curvature, and has no significant effect on accuracy. Therefore, it can be used directly to describe the relationship between the interlayer pressure and interlayer distance in FEM simulations and has been used in ABAQUS/Explicit as a basis for defining the normal interaction between the inner and outer tubes.

For the tangential force equivalence, the axial pull-out process of four 10.084 nm-long (5,5)/(10,10) DWCNTs with different numbers of missing atoms at the ends of the outer walls was simulated (Fig. 7). The left end of the outer wall was axially fixed (x-axis) and the right end of the inner wall was axially pulled out with a constant speed of 20 m/s. The relationship between the axial pull-out force and displacement is plotted in Fig. 8. Similar to the previous reports [9,27], the pull-out process of the inner wall can be divided into three stages. Firstly, the pull-out force increases sharply with the increase in displacement. Then, for large displacements, the pull-out force maintains a slight periodic up-and-down motion around 1.2 nN, which is caused by the repetitive destruction and forming of vdW forces as the inner wall slides. Finally, the pull-out force decreases rapidly. Therefore, in FEM simulations, we apply a pair of opposing tangential forces of 1.2 nN at the circumference of the ends of the inner and outer tubes.

Moreover, in Fig. 8, it can be found the pullout force–displacement curves almost coincide, but differ slightly in the final stage. The pullout force of DWCNTs with non-straight fracture configuration decreases slowly in advance, because the large atomic deficiency causes an imbalance of the vdW force in the cross-section. In general, the fracture configuration plays a small role in the interwall interaction compared to the effect of atoms missing in the middle of the outer wall [27], which causes a large fluctuation in the pull-out force. Therefore, we just consider the straight fracture configuration without any vacancy defects in the subsequent simulations.

Meanwhile, a large number of experimental or simulation studies [14,17,45,46] have shown that the inter-layer interaction of carbon nanotubes mainly originates from the ends of the carbon nanotubes, regardless of the overlap length between the tube layers. Combining the results of the above MD simulations and previous studies, a pair of opposing tangential vdW forces are applied to the circumference of the inner and outer tube ends, respectively, as the equivalent of the tangential interaction in the FEM simulations.

To verify the reliability of the above equivalents, we performed the lateral loading of 30 nm-long DWCNTs by FEM. The deformation of the nanotube simulated by FEM (Fig. 9a) is similar to that simulated by MD (Fig. 5b). And the lateral load–displacement curves obtained by MD and FEM match well (Fig. 9b). Both of them prove that the FEM simulations are reliable. The effect of the initial gap length (l) between the left and right outer tubes is also investigated. Taking the 30 nm-long DWCNTs as an example, the influence of the initial gap length l between the left and right outer tubes is simulated by FEM. Two initial gap lengths are considered: $l = 0.1$ nm and $l = 1.0$ nm. Simulation results show that the influence of the initial gap length is small (Fig. 10).

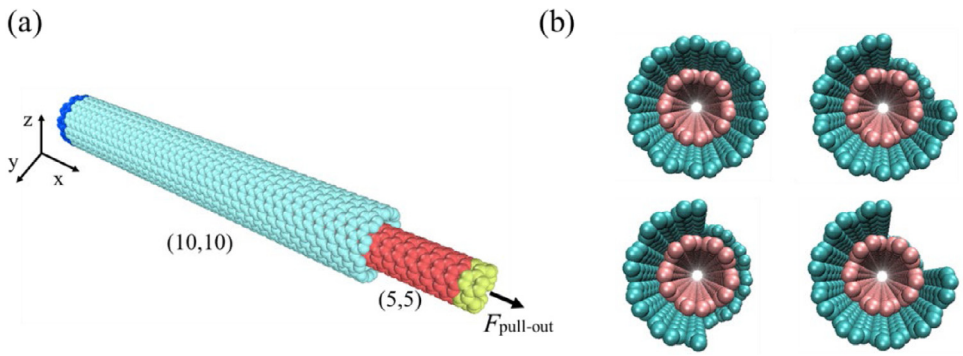

Fig. 7. (a) MD model simulates the pull-out of (5,5)/(10,10) DWCNTs, and (b) four fracture configurations: without vacancy defect, with 1/4 and 1/2 of the atoms missing in the length range of 1 nm from the end, and with 1/4 of the atoms missing in the length range of 2 nm from the end.

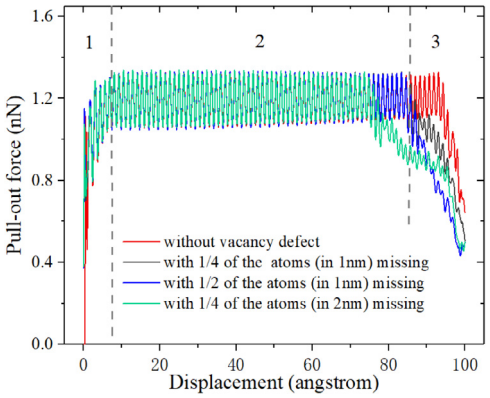

Fig. 8. Relationship between the axial pull-out force and displacement of four (5,5)/(10,10) DWCNTs.

Four longer (5,5)/(10,10) DWCNTs with lengths of 40 nm, 60 nm, 80 nm, and 100 nm are then simulated with FEM for lateral loading. The results show that for length L < 60 nm, sliding and buckling occur synchronously; while for L > 60 nm, the inner tube slides first and then the outer tube buckles (Fig. 13b). This phenomenon is consistent with the results of MD simulations. The lateral force–displacement curves obtained by FEM are also compared with the MD results (Fig. 11). The peak force (buckling force) gradually decreases as the length of DWCNTs increases. When the critical length is reached, the peak force on the lateral force–displacement curve disappears, and the steady pull-out force tends to a limit value F_{const} (shown by the black line).

3.3. Effect of CNT length on lateral pull-out force

To study the effect of nanotube length on the pull-out force, we also load (5,5)/(10,10) DWCNTs with lengths of 20 nm, 40 nm, and 60 nm. For DWCNTs with lengths of 20–40 nm, the trend of their lateral force–displacement curves, as shown in Fig. 12, is consistent, while the maximum lateral forces (peak forces) and the stable lateral forces vary with the nanotube lengths. As the tube length increases, the lateral force at the onset of the buckling decreases. For DWCNTs with a length of 60 nm, the force peak disappears.

The geometries of the critical buckling are shown in Fig. 13a. We find that these geometries are similar and the critical buckling curvature κ_{cr} is approximately equal to 0.05 nm^{-1}, indicating that κ_{cr} is not sensitive to the nanotube length. For DWCNTs with lengths of 20–40 nm, the buckling of outer tubes occurs synchronously with the sliding of inner tubes. And also, the buckling positions of the outer tube (shown by purple solid arrows) coincide with the roots of the inner tube (shown by red dotted arrows). While for the 60 nm-long DWCNTs, the inner tube slides first, and then the outer tube buckles. The buckling positions of the outer tube do not overlap with the roots of the inner tube. Moreover, only the outer tube buckling can be observed in the MD and FE simulation. This is because that the position of the inner tube is always in the state of a double walled tube, while the outer tube is in the state of a single walled tube when the inner tube slides away. Because the effective thickness at the position of the DWCNTs is greater than that at the position of the single walled carbon tubes, only the outer tube buckles under the lateral loading.

3.4. Critical lateral force and Critical length

To explain the above lateral force–displacement curves, theoretical analyses were carried out for Stages I and II.

Theory for Stage I

The above MD and FEM results show that the outer tubes were bent in Stage I. Assuming that the carbon nanotube is a continuous beam, the bending moment at the root of the outer tube is

$$M = \frac{FL}{4} \tag{1}$$

where F is the lateral concentration force in the middle and L is the tube length. Yakobson et al. [42] derived that the critical bending buckling curvature of carbon nanotubes κ_{cr} is $\frac{4h}{\sqrt{3}\sqrt{1-\nu^2}}\frac{1}{d^2}$, where h is the effective mechanical wall thickness ($h = 0.066$ nm), ν is the Poisson's ratio ($\nu = 0.19$), and d is the diameter. Considering that critical bending moment $M_{cr} = EI\kappa_{cr}$, we can obtain the critical lateral force

$$F_{cr} = \frac{4EI\kappa_{cr}}{L} = \frac{16Elh}{\sqrt{3}\sqrt{1-\nu^2}}\frac{1}{d^2L} \tag{2}$$

where E is the effective Young's modulus ($E = 5.15$ TPa) and the inertia moment of the tube I equals $\frac{\pi}{64}((d+h)^4 - (d-h)^4)$ [43]. For the outer (10,10) tube, κ_{cr} equals to $0.155(\text{nm})/d^2$, and then the critical lateral force (critical buckling force) is

$$F_{cr} = \frac{112.66(\text{nN}\cdot\text{nm})}{L} \tag{3}$$

Theory for Stage II

After the outer tube buckles, the configuration of the tube at the buckling position is similar to a plastic hinge as shown in Fig. 14. Furtherly, taking the 100 nm-long DWCNTs as an example, the bending moment at the root of the outer tube during lateral loading is obtained by FEM (Fig. 15). After the outer tube buckles, the bending moment at the root of the outer

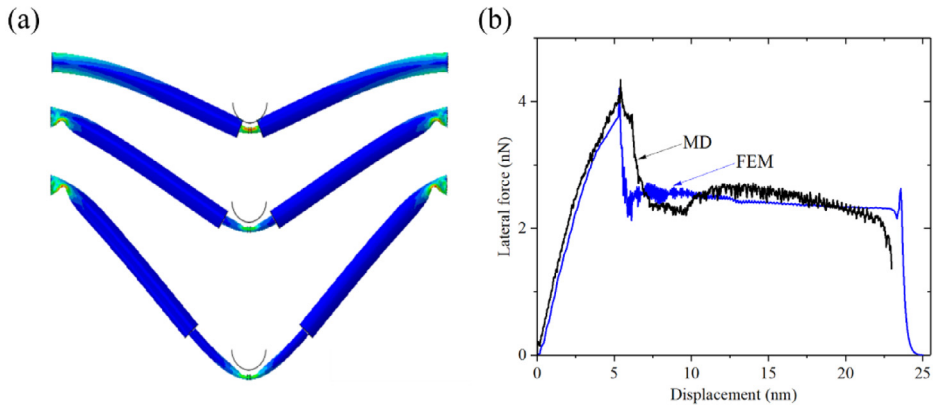

Fig. 9. FEM results, (a) deformation of a 30 nm-long DWCNTs, and (b) lateral force–displacement of a 30 nm-long DWCNTs obtained by FEM and MD, respectively.

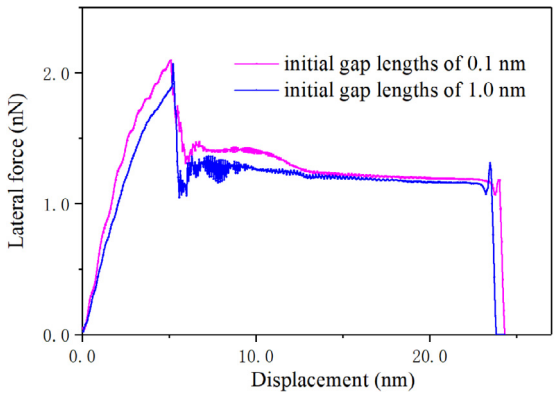

Fig. 10. 10. Lateral force–displacements for DWCNTs with initial gap lengths of 0.1 nm and 1.0 nm.

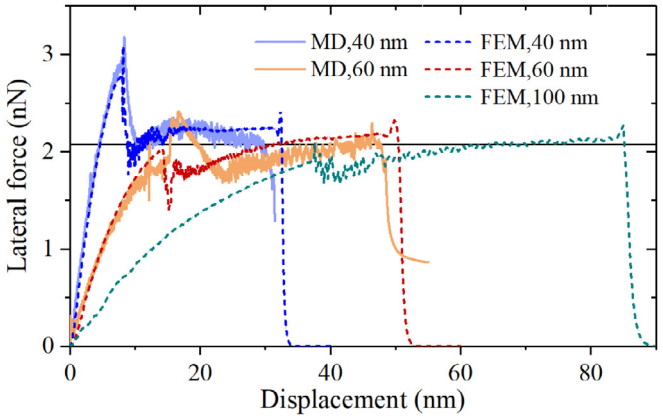

Fig. 11. Comparison of lateral force–displacement curves of (5,5)/(10,10) DWCNTs obtained by MD and FEM.

tube is almost constant. Thus, the tube at the buckling position can be considered as a plastic hinge. As the lateral displacement increases, the outer tube rotates only around the hinge, and then the lateral displacement of the outer tube is

$$u_1 = (x - \frac{L}{2})\cot\theta,\ \frac{L}{2}(1-\sin\theta) \le x < \frac{L}{2} \tag{4}$$

where θ is the angle between the tube axis and the u-axis.

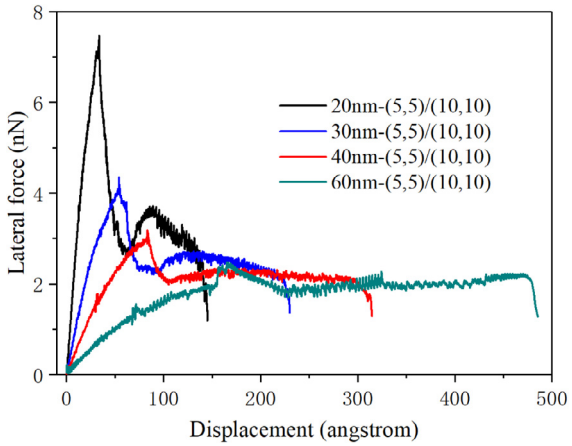

Fig. 12. Lateral force–displacement curves of (5,5)/(10,10) DWCNTs with different lengths.

Assuming that the inner tube is an Euler–Bernoulli beam, it satisfies the equation

$$\frac{\partial^2}{\partial x^2}(EI\frac{\partial^2 u_2}{\partial x^2}) = 0 \tag{5}$$

Thus, it can be assumed that the lateral displacement of the inner tube is

$$u_2 = \frac{M}{2EI}x^2 - a,\ 0 \le x < \frac{L}{2}(1-\sin\theta) \tag{6}$$

Considering that the intersection of the inner and outer tubes satisfies two boundary continuity conditions, i.e., continuity of displacement and continuity of angle (Eq. (8)), we can obtain the parameter based on the force analysis performed on the outer and inner tubes after the buckling of the outer tube occurred (Stage II), as shown in Fig. 16.

$$a = \frac{1}{2}L\cos\theta + \frac{1}{4}L\cot\theta(1-\sin\theta) \tag{7}$$

The equations corresponding to the continuity of displacement and the continuity of angle are

$$y_1\left(\frac{L}{2} - \frac{L}{2}\sin\theta\right) = y_2\left(\frac{L}{2} - \frac{L}{2}\sin\theta\right) \tag{8.1}$$

$$y_1'\left(\frac{L}{2} - \frac{L}{2}\sin\theta\right) = y_2'\left(\frac{L}{2} - \frac{L}{2}\sin\theta\right) \tag{8.2}$$

We conduct the force analysis on the outer and inner tubes separately shown in Fig. 16. The bending moment at the root of

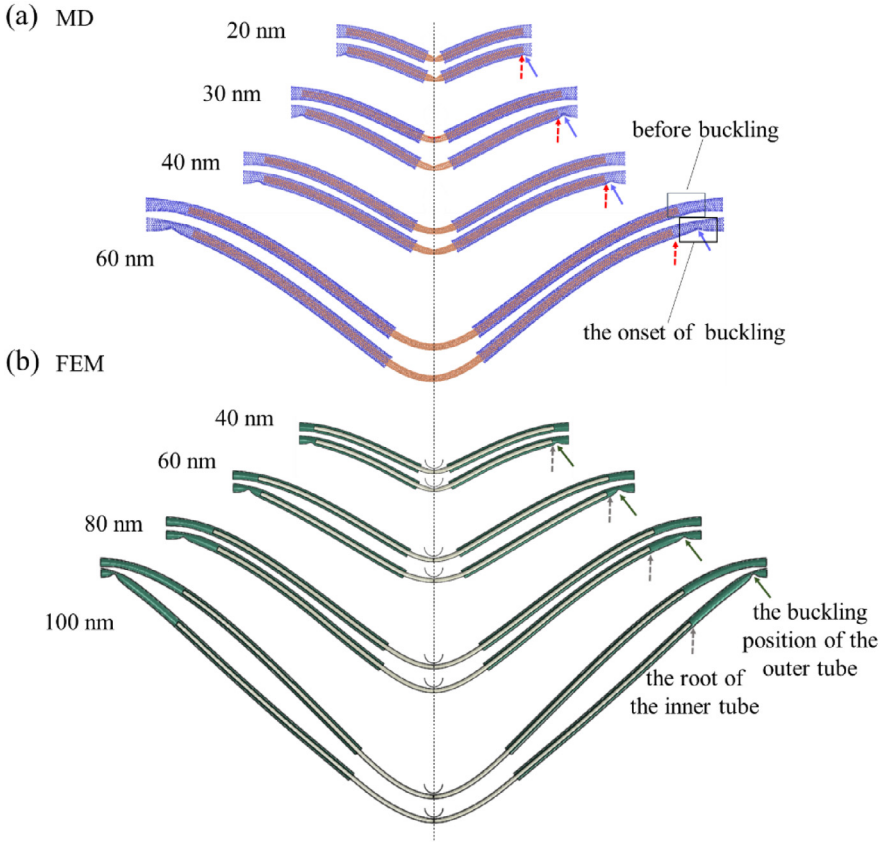

Fig. 13. Geometries of (5,5)/(10,10) DWCNTs with different lengths before buckling (the upper one for each length) and at the onset of buckling (the lower one for each length) as simulated by (a) MD and (b) FEM. The solid arrows refer to the buckling positions of the outer tubes. The dotted arrows refer to the roots of the inner tubes.

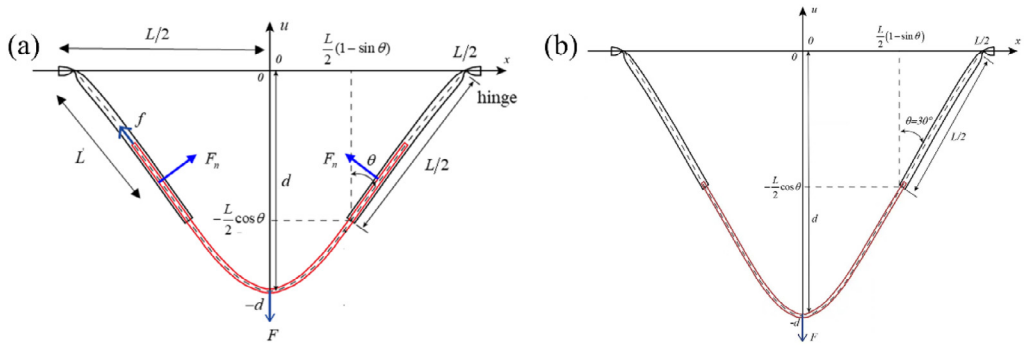

Fig. 14. (a) Configuration and force analysis of the theoretical model after the outer tube buckled. (b) The final state when the inner tube is just completely pulled out from the outer tube.

the outer tube is

$$M_{root} = F_n L' \tag{9}$$

where F_n is the equivalent normal force perpendicular to the tube axis and L' is the equivalent length of the force arm (Fig. 14). The FEM analysis shows that M_{root} is almost unchanged after the outer tube buckled as shown in Fig. 15. The theoretical lateral force can be written as

$$\begin{aligned} F &= 2f\cos\theta + 2F_n \sin\theta \\ &= 2f\cos\theta + 2\frac{M_{root}}{\frac{1}{2}\sqrt{(\frac{L}{2})^2+d^2}}\sin\theta \end{aligned} \tag{10}$$

where f is the vdW force and M_{root} is the bending moment at the root of the outer tube. By MD simulation illustrated in Fig. 8 and discussion in Section 3.2, f is set as 1.2 nN in this study because the pull-out force is around 1.2 nN as the inner tube is gradually pulled out from the outer tube. The bending moment M_{root}, as discussed in Section 3.4, it is calculated by FEM and is shown in Fig. 15. It can be found that the bending moment is almost constant after the outer tube buckled. Thus, M_{root} is set as $7.5 * 10^{-18}$ J in this study. In Eq. (10), the first term increases as θ decreases, while the second term decreases as θ decreases. They result in the lateral pull-out force remaining almost constant with the increase of displacement. Based on the above theory, we observe that the theoretical predictions agree well with FEM results (Fig. 17).

Comparison between MD, FEM, and theory

The MD and the FEM results were compared with the theoretical results of Stages I and II (Fig. 19). Fig. 19 shows that the above theories can accurately predict the peak lateral force.

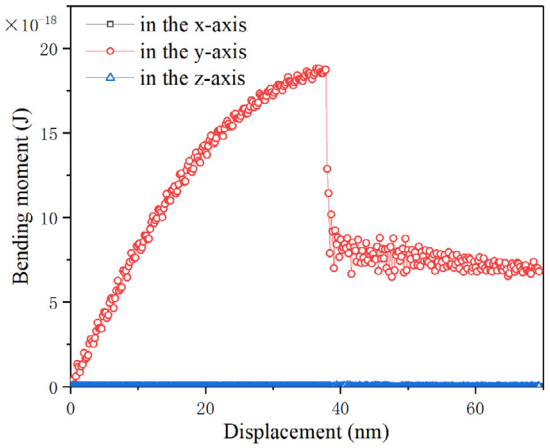

Fig. 15. Bending moment-displacement curve of a 100 nm-long DWCNTs.

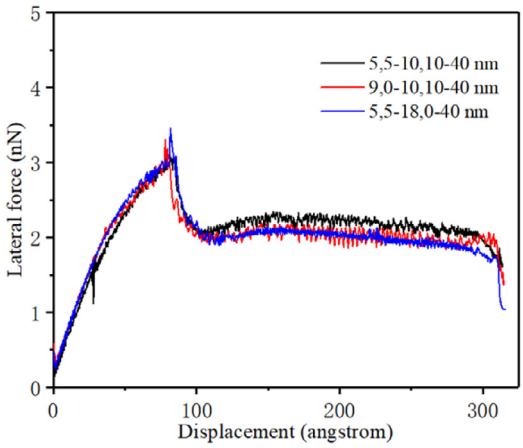

Fig. 18. Atomistic calculations of the lateral force–displacement for four typical chirality systems.

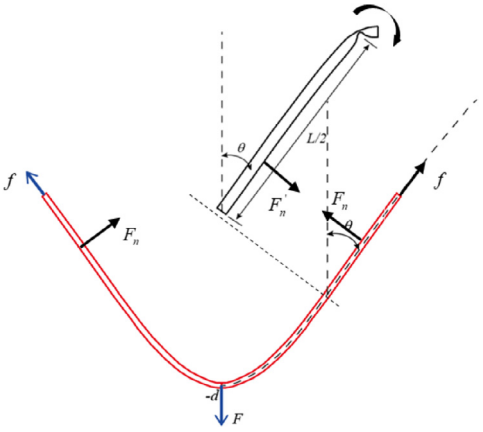

Fig. 16. Force analysis for the outer and the inner tubes.

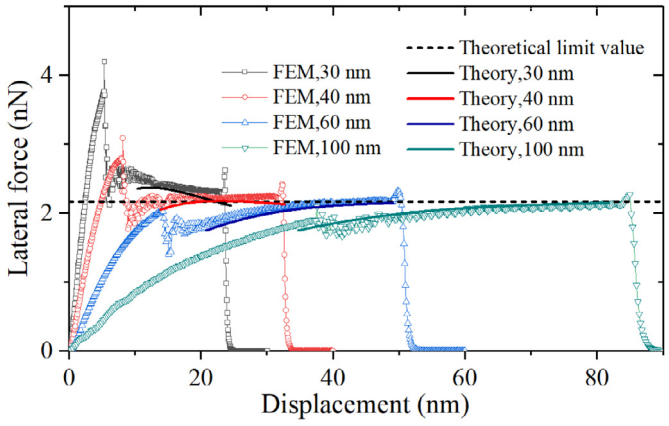

Fig. 17. Comparison of lateral force–displacement curves obtained from FEM and theory in Stage II.

For (5,5)/(10,10) DWCNTs, the theoretical critical length L_{cr} is 54.2 nm. At this point, the critical lateral force of Stage I is equal to the stable lateral force of Stage II. The stable lateral force is independent of the length and tends to be 2.08 nN. This is because the theoretical lateral force as shown in Eq. (10) consists of two parts: the first part is resulted from the vdW force and the second part is caused by the bending moment. For the first part, f equals to 1.2 nN as discussed in Fig. 8. For the second part, M_{root} is close to $7.5^{*}10^{-18}$J after the outer tube buckled as discussed in Fig. 15. Therefore, with the increase of the θ, the first part decreases, while the second part increases. The final state, as shown in Fig. 14(b), is that the inner tube is just completely pulled out from the outer tube, where θ is 30° in the triangle composed of the x-axis, the y-axis and the hypotenuse formed by the inner and outer tubes. This is because the length of the Cathetus in the x-axis is $L/2$, while the length of the hypotenuse is L when the inner tube is just completely pulled out from the outer tube. As a result, the first part is 2.08 nN, while the second part approaches zero when the length of the CNTs becomes infinite. The magnitude of the force jump (F_{jump}) gradually decreases as the length of the nanotube increases, where F_{jump} is the difference between the critical lateral force and the stable lateral force. When the length is greater than the critical length L_{cr}, F_{jump} drops to about zero. In addition, the effect of chirality was investigated by lateral loading (5,5)/(10,10) armchair/armchair (A–A), (9,0)/(10,10) zigzag/armchair (Z–A), and (5,5)/(18,0) armchair/zigzag (A–Z) DWCNTs with same lengths of 40 nm. As shown in Fig. 18, when the displacement is greater than a critical value, the lateral force tends to be constant, but has different fluctuation amplitudes. For a stable load segment, the force fluctuation amplitudes of the four systems are proportional to the ratio of 2.3: 3.0:1.0. The force fluctuation of a perfect bi-tube system depends to a large extent on the commensuration. Theoretical calculations show that two layers of graphite sheets in contact in the commensurate mode have higher interaction energy than graphite sheets in contact with other incommensurate forms. This means that the interaction force between the commensurate graphite sheets is significantly greater than that of the incommensurate ones. As the DWCNTs are composed of coaxial cylindrical graphene layers, the above lattice matching concept is also applicable to the interaction between the walls of DWCNTs. When the chiral index of the inner wall and outer wall are A–A type, they can satisfy the commensurate AB stacking state. Such a conclusion, that the incommensurate Z–A/A–Z types are found to be much smoother than a commensurate A–A type, is consistent with experimental and simulated results of relative sliding of the inner and outer walls of DWCNTs [36,37] and the sliding of small graphite flakes on graphite substrates. The results show that the critical lateral force is insensitive to these three different types of chirality.

4. Conclusions

We performed the pull-out experiments of individual DWCNTs by lateral loading under an optical microscope, conducted

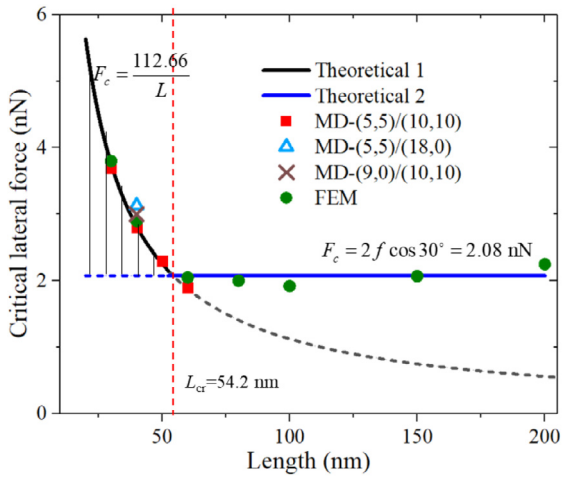

Fig. 19. The comparison between MD, FEM and theoretical results.

corresponding MD and FEM simulations based on reasonable equivalents, and proposed a detailed theoretical model to describe the pull-out process. Several conclusions can be drawn as follows.

(1) The sudden force drop in the lateral force–displacement curve is due to the local snap buckling of the outer walls near the fixed ends.

(2) The critical length related to the diameter is 54.2 nm for the DWCNTs with the outer tube diameter of 0.955 nm studied in this paper. The results show that for L < 54.2 nm, the buckling of the outer tube and the sliding of the inner tube occur simultaneously. For L > 54.2 nm, the sliding of the inner tube occurs before the buckling of the outer tube.

(3) The stable lateral force is independent of the length of the DWCNTs and tends to be equal to 2.08 nN.

The theoretical model and numerical results in this paper have potential applications, such as the study of interwall interaction behavior of multilayer CNTs (greater than or equal to three layers) under lateral loading, and the study of lateral deformation behavior of multilayer graphene. Moreover, to validate the theoretical and numerical models proposed in this study, the sliding behavior of DWCNTs with different lengths under lateral loading will be experimentally investigated in the high-resolution electron microscopy in our future work.

Declaration of competing interest

The authors declare that they have no known competing financial interests or personal relationships that could have appeared to influence the work reported in this paper.

Data availability

Data will be made available on request.

Acknowledgments

This work was supported by the National Natural Science Foundation of China (No. 11902311, 121721901, 1872035, 12272203, 12302236, 11632010, 12022210, 12032001), by Youth Innovation Promotion Association CAS, China (2018022), and by Foundation of China Academy of Railway Sciences Corporation Limited (2019YJ153).

References

[1] K. Koziol, et al., High-performance carbon nanotube fiber, Science 318 (2007) 1892–1895.
[2] A.B. Dalton, et al., Super-tough carbon-nanotube fibres, Nature 423 (2003) 703.
[3] A. Cao, P.L. Dickrell, W.G. Sawyer, M.N. Ghasemi-Nejhad, P.M. Ajayan, Super-compressible foamlike carbon nanotube films, Science 310 (2005) 1307–1310.
[4] J.-L. Zang, Y.-P. Zhao, Silicon nanowire reinforced by single-walled carbon nanotube and its applications to anti-pulverization electrode in lithium ion battery, Composites B 43 (2012) 76–82.
[5] S. Iijima, Helical microtubules of graphitic carbon, Nature 354 (1991) 56–58.
[6] Y. Saito, T. Yoshikawa, S. Bandow, M. Tomita, T. Hayashi, Interlayer spacings in carbon nanotubes, Phys. Rev. B 48 (1993) 1907–1909.
[7] Q. Zheng, Q. Jiang, Multiwalled carbon nanotubes as gigahertz oscillators, Phys. Rev. Lett. 88 (2002) 045503.
[8] J. Cumings, A. Zettl, Low-friction nanoscale linear bearing realized from multiwall carbon nanotubes, Science 289 (2000) 602–604.
[9] Y. Li, et al., Molecular mechanics simulation of the sliding behavior between nested walls in a multi-walled carbon nanotube, Carbon 48 (2010) 2934–2940.
[10] A.M. Fennimore, et al., Rotational actuators based on carbon nanotubes, Nature 424 (2003) 408–410.
[11] K.T. Chan, Y. Zhao, The dispersion characteristics of the waves propagating in a spinning single-walled carbon nanotube, Sci. China Phys. Mech. Astron. 54 (2011) 1854.
[12] M.-F. Yu, B.I. Yakobson, R.S. Ruoff, Controlled sliding and pullout of nested shells in individual multiwalled carbon nanotubes, J. Phys. Chem. B 104 (2000) 8764–8767.
[13] M.-F. Yu, et al., Strength and breaking mechanism of multiwalled carbon nanotubes under tensile load, Science 287 (2000) 637–640.
[14] A. Kis, K. Jensen, S. Aloni, W. Mickelson, A. Zettl, Interlayer forces and ultralow sliding friction in multiwalled carbon nanotubes, Phys. Rev. Lett. 97 (2006) 025501.
[15] T. Filleter, et al., Experimental-computational study of shear interactions within double-walled carbon nanotube bundles, Nano Lett. 12 (2012) 732–742.
[16] R. Zhang, et al., Superlubricity in centimetres-long double-walled carbon nanotubes under ambient conditions, Nat. Nanotech. 8 (2013) 912–916.
[17] R. Zhang, et al., Interwall friction and sliding behavior of centimeters long double-walled carbon nanotubes, Nano Lett. 16 (2016) 1367–1374.
[18] R. Yazdanparast, R. Rafiee, Investigating the influence of pull-out speed on the interfacial properties and pull-out behavior of CNT/polymer nanocomposites, Compos. Struct. 316 (2023) 117049.
[19] R. Rafiee, M. Sharaei, Investigating the influence of bonded and non-bonded interactions on the interfacial bonding between carbon nanotube and polymer, Compos. Struct. 238 (2020) 111996.
[20] Z. Xia, W.A. Curtin, Pullout forces and friction in multiwall carbon nanotubes, Phys. Rev. B 69 (2004) 233408.
[21] D. Qian, W.K. Liu, R.S. Ruoff, Load transfer mechanism in carbon nanotube ropes, Compos. Sci. Technol. 63 (2003) 1561–1569.
[22] R. Mirzaeifar, Z. Qin, M.J. Buehler, Mesoscale mechanics of twisting carbon nanotube yarns, Nanoscale 7 (2015) 5435–5445.
[23] D. Qian, G.J. Wagner, W.K. Liu, M.-F. Yu, R. Ruoff, Mechanics of carbon nanotubes, Appl. Mech. Rev. 55 (2002) 495–533.
[24] P. Tangney, S.G. Louie, M.L. Cohen, Dynamic sliding friction between concentric carbon nanotubes, Phys. Rev. Lett. 93 (2004) 065503.
[25] J. Servantie, P. Gaspard, Methods of calculation of a friction coefficient: Application to nanotubes, Phys. Rev. Lett. 91 (2003) 185503.
[26] Z. Guo, T. Chang, X. Guo, H. Gao, Thermal-induced edge barriers and forces in interlayer interaction of concentric carbon nanotubes, Phys. Rev. Lett. 107 (2011) 105502.
[27] X. Yuan, Y. Wang, Atomistic simulations on interwall sliding behaviour of double-walled carbon nanotube: Effects of structural defects, Mol. Simul. 43 (2017) 953–961.
[28] S.K. Pregler, S.B. Sinnott, Molecular dynamics simulations of electron and ion beam irradiation of multiwalled carbon nanotubes: The effects on failure by inner tube sliding, Phys. Rev. B 73 (2006) 224106.
[29] M. Liu, et al., Strength and fracture behaviors of ultralong carbon nanotubes with defects, Carbon 199 (2022) 300–317.
[30] Y. Bai, et al., Carbon nanotube bundles with tensile strength over 80 GPa, Nat. Nanotech. 13 (2018) 589–595.
[31] M. Liu, et al., Multi-scale analysis of the interaction in ultra-long carbon nanotubes and bundles, J. Mech. Phys. Solids 142 (2020) 104032.

[32] X. Ye, Z. Cui, H. Fang, X. Li, A multiscale material testing system for in situ optical and electron microscopes and its application, Sensors 17 (2017) 1800.
[33] Y. Bai, et al., Super-durable ultralong carbon nanotubes, Science 369 (2020) 1104–1106.
[34] R. Zhang, et al., Superstrong ultralong carbon nanotubes for mechanical energy storage, Adv. Mater. 23 (2011) 3387–3391.
[35] X. Ye, T. Wang, Z. Zhuang, X. Li, Tensile properties of individual multi-cellular Bacillus subtilis fibers, Sci. China Phys. Mech. Astron. 62 (2019) 994611.
[36] B. Bourlon, D.C. Glattli, C. Miko, L. Forró, A. Bachtold, Carbon nanotube based bearing for rotational motions, Nano Lett. 4 (2004) 709–712.
[37] W. Guo, Y. Guo, H. Gao, Q. Zheng, W. Zhong, Energy dissipation in gigahertz oscillators from multiwalled carbon nanotubes, Phys. Rev. Lett. 91 (2003) 125501.
[38] S.J. Stuart, A.B. Tutein, J.A. Harrison, A reactive potential for hydrocarbons with intermolecular interactions, J. Chem. Phys. 112 (2000) 6472–6486.
[39] R. Rafiee, M. Mahdavi, Characterizing nanotube–polymer interaction using molecular dynamics simulation, Comput. Mater. Sci. 112 (2016) 356–363.
[40] R. Rafiee, M. Mahdavi, Molecular dynamics simulation of defected carbon nanotubes, Proceed. Inst. Mech. Eng. Part L J. Mater. Des. Appl. 230 (2016) (2016) 654–662.
[41] T.A. Halgren, The representation of van der waals (vdW) interactions in molecular mechanics force fields: Potential form, combination rules, and vdw parameters, J. Am. Chem. Soc. 114 (1992) 7827–7843.
[42] B.I. Yakobson, C.J. Brabec, J. Bernholc, Nanomechanics of carbon tubes: Instabilities beyond linear response, Phys. Rev. Lett. 76 (1996) 2511–2514.
[43] J. Wang, et al., The applicability and the low limit of the classical fracture theory at nanoscale: The fracture of graphene, Eng. Fract. Mech. 284 (2023) 109282.
[44] A. Pantano, D. M. Parks, M.C. Boyce, Mechanics of deformation of single- and multi-wall carbon nanotubes, J. Mech. Phys. Solids 52 (2004) 789–821.
[45] D. Xia, et al., Extracting the inner wall from nested double-walled carbon nanotube by platinum nanowire: Molecular dynamics simulations, RSC Adv. 7 (2017) 39480–39489.
[46] G. Yamamoto, et al., Prediction of pull-out force of multi-walled carbon nanotube (MWCNT) in sword-in-sheath mode, Comput. Mater. Sci. 60 (2012) 7–12.